Overview of MAST Results

G.F. Counsell 1), R.J. Akers 1), L.C. Appel 1), D. Applegate 2), K.B. Axon 1), Y. Baranov 1), C. Brickley 1), C. Bunting 1), R.J. Buttery 1), P.G. Carolan 1), C. Challis 1), D. Ciric 1), N.J. Conway 1), M. Cox 1), G. Cunningham 1), A. Darke 1), A. Dnestrovskij 3), J. Dowling 1), B. Dudson 4), M.R. Dunstan 1), E. Delchambre 1), A.R Field 1), A Foster 5), S. Gee 1), M.P. Gryaznevich 1), P. Helander 1), T.C. Hender 1), M. Hole 1), D.H. Howell 1), N. Joiner 2), D. Keeling 1), A. Kirk 1), I.P. Lehane 6), S. Lisgo 1), B. Lloyd 1), F. Lott 2), G.P. Maddison 1), S.J. Manhood 1), R. Martin 1), G.J. McArdle 1), K.G. McClements 1), H. Meyer 1), A.W. Morris 1), M. Nelson 7), M. R. O'Brien 1), A. Patel 1), T. Pinfold 1), J Preinhaelter 8), M.N. Price 1), C.M. Roach 1), V. Rozhansky 9), S. Saarelma 1), A. Saveliev 10), R. Scannell 6), S. Sharapov 1), V. Shevchenko 1), S. Shibaev 1), K. Stammers 1), J. Storrs 1), A. Sykes 1), A. Tabasso 1), S. Tallents 2), D. Taylor 1), M.R. Tournianski 1), A. Turner 1), G. Turri 2), M. Valovic 1), F. Volpe 1), G. Voss 1), M.J. Walsh 11), J.R. Watkins 1), H.R. Wilson 1), M. Wisse 6) and the MAST, NBI and ECRH Teams.

1) EURATOM/UKAEA Fusion Association, Culham Science Centre, Abingdon, Oxfordshire OX14 3DB, UK
2) Imperial College, Prince Consort Road, London SW7 2BZ, UK
3) Kurchatov Institute, Moscow, Russia
4) Oxford University, Clarendon Laboratory, Parks Road, Oxford, OX1 3PU, UK
5) University of Strathclyde, Glasgow, G4 0NG, UK
6) University College, Cork, Ireland
7) Queens University, Belfast, BT7 1NN, UK
8) EURATOM/IPP.CR Fusion Association, Institute of Plasma Physics, Prague, Czech Republic
9) St. Petersburg State Politechnical University, Polytechnicheskaya 29, 195251 St. Petersburg, Russia
10) A.F. Ioffe Physico-Technical Institute, St. Petersburg, Russia
11) Walsh Scientific Ltd, Culham Science Centre, Abingdon, OX14 3EB, UK

E-mail: glenn.counsell@ukaea.org.uk

Abstract

Significant progress has been made on MAST towards a fundamental understanding of transport, stability and edge physics and addressing technological issues for future large devices. Collaborative studies of the L-H transition with NSTX and ASDEX Upgrade confirm that operation in a connected double-null configuration significantly reduces the threshold power, P_{thr}. MAST data provide support for a theory for the transition based on finite β drift wave turbulence suppression by self-generated zonal flows. Analysis of low and high field side density gradients in the H-mode pedestal provide support for an analytical model of the density pedestal width dependent on the neutral penetration depth. Adding MAST data to international confinement databases has enhanced confidence in scalings for ITER by significantly expanding the range of β and ε explored and indicates a slightly stronger ε dependence than in current scalings. Studies of core transport have been conducted for well diagnosed, L-mode, H-mode and ITB discharges using TRANSP and microstability and turbulence studies have been carried out using GS2. Linear micro-stability analysis indicates that ITG modes are typically unstable on all flux surfaces with growth rates that are comparable to the equilibrium **ExB** flow shearing rate. Mixing length estimates of transport coefficients from ITG (neglecting flow shear) give diffusion coefficients that are broadly comparable with observed thermal diffusivities. Non-linear, collisionless ETG calculations have been performed and suggest radially extended electrostatic streamers up to $100\rho_e$ across in radius. Transport from ITG could easily be suppressed in regions where the **ExB** shear flow rate, ω_{SE} exceeds the ITG growth rate, possibly contributing to ITBs. Toroidal rotation, driven by neutral beam torque, is the

dominant contribution to ω_{SE} via the $v_\phi B_\theta$ term in the radial electric field. Early ELM activity on MAST is associated with the formation of narrow filamentary structures following field lines in the edge. These filaments rotate toroidally with the edge plasma and, away from the X-points, accelerate radially outwards from the edge up to 20cm. Studies of disruptions on MAST demonstrate a complex evolution of core energy loss and resultant divertor power loads, including phases where the target heat flux width is broadened by a factor 8. Observations of energetic particle modes driven by super-Alfvénic beam ions provide support for a model for the non-linear evolution of toroidal Alfvén eigenmodes (AE) forming BGK waves. AE activity reduces to low levels with increasing β. Plasma start-up without a central solenoid and in a manner compatible with future large ST devices has been demonstrated using breakdown at a quadrupole magnetic null. Closed flux surface plasmas with peak plasma currents up to 370 kA have been generated and sustained for 0.3s. New error field correction coils have extended the operational space for low density plasmas and enabled scaling studies of error field induced locked mode formation in the ST.

1. Introduction

Experiments and modelling on the Mega Ampere Spherical Tokamak (MAST) at UKAEA Fusion are focused on the core goals of improving fundamental understanding of transport, stability and edge physics and investigating technological solutions to heating, current drive and plasma exhaust, both for ITER and future spherical tokamak (ST) devices. This paper presents an overview of recent experimental results, analysis and modelling on MAST in a number of these core areas. Section 2 discusses the nature of the L-H transition and H-mode pedestal in MAST and reviews the contribution of MAST data to international efforts aimed at predicting H-mode energy confinement times in ITER, highlighting the impact on scalings of extensions to the parameter space afforded by the low aspect ratio and high normalised plasma pressure in MAST. Section 3 describes the use of gyro-kinetic, fluid, Monte-Carlo and combined codes to model particle and energy transport in the core and edge of MAST, focussing in particular on pairs of 'matched' L-mode/H–mode and Co-NBI/Counter-NBI ITB plasmas for which well validated, high quality experimental data is available. Finally, Section 4 explores the nature of transient phenomena in MAST, concentrating on the structure of perturbations to the magnetic equilibrium during the earliest phases of edge-localised modes and on the spatial distribution of energy released during plasma disruptions, and additionally discusses observations of energetic particle modes driven by the super-Alfvénic, fast ion population in MAST. Section 5 addresses the ST-specific issue of plasma start-up without the use of a central solenoid, which will not be allowable in a high neutron flux ST, and discusses efforts to extend the operational space for MAST plasmas towards regimes compatible with full, non-inductive current drive and to develop steady-state plasma exhaust schemes compatible with future large ST devices.

2. Global Confinement

2.1. The L-H Transition

Common theories attempting to explain the L-H transition have been challenged by observations on MAST, supported by comparison studies on ASDEX Upgrade and NSTX, of a significant decrease in P_{thr} for equilibrium configurations close to connected double-null (CDN) [1,2]. In the ST devices (MAST and NSTX) the reduction in P_{thr} is a factor 2 or more compared to operation in similarly shaped, single-null plasmas with the ion ∇B drift towards the X-point (LSN). In ASDEX Upgrade the effect is less, a factor 1.2 - 1.25, [3] even for plasmas with elongation, triangularity and minor radius well matched to a typical MAST equilibrium and is only observed when the plasma is maintained in a very accurate CDN configuration. The strong sensitivity of the effect to the accuracy of the double-null may explain why other devices have reported a minimum in P_{thr} for the LSN configuration rather than for CDN.

Although the CDN configuration modifies P_{thr} significantly, there is little impact on edge temperature and density profiles in L-mode with changes between CDN and similar shape single null configurations. Only the toroidal rotation velocity of impurity ions, which is related to the edge radial electric field, shows any noticeable change. The period immediately following L-H transitions in configurations close to CDN on MAST shows rather different ELM characteristics, exhibiting a gradual evolution through rapid type III ELMs rather than an abrupt transition into an ELM-free phase, which is observed in LSN even at power levels close to P_{thr}. A study of the impact of equilibrium changes between LSN and CDN using the ELITE linear ideal-MHD stability code [3,4] does not reveal any

significant difference in growth rates for intermediate-n peeling-ballooning modes. This suggests that the ELM-free behaviour following the L-H transition in LSN plasmas is due to a mechanism that prevents the edge pressure profile from reaching the stability boundary. Identification of this mechanism will require further investigation of LSN plasmas with higher auxiliary heating.

Predictions for the L and H-mode existence space in MAST were tested for four leading L-H transition theories [3] against a database of MAST plasmas for which high spatial resolution density and temperature profiles exist. A reasonable qualitative fit to the MAST data was only obtained for a theory based on finite β drift wave turbulence suppression by self-generated zonal flows [5], which predicts the existence of an H-mode in plasmas with $T_\psi > T_{EC}$ (figure 1). T_ψ is the electron temperature at the pedestal (or corresponding flux surface in L-mode). T_{EC} is given by $T_{EC} = CB_\phi^{2/3} Z_{eff}^{1/3} L_n^{1/2} R^{-1/6} M^{-1/6}$, where Z_{eff} is the effective atomic number, M is the mass of the principal species and L_n is the edge density gradient length. The constant used in this work, C=1 is a factor 1/0.45 larger
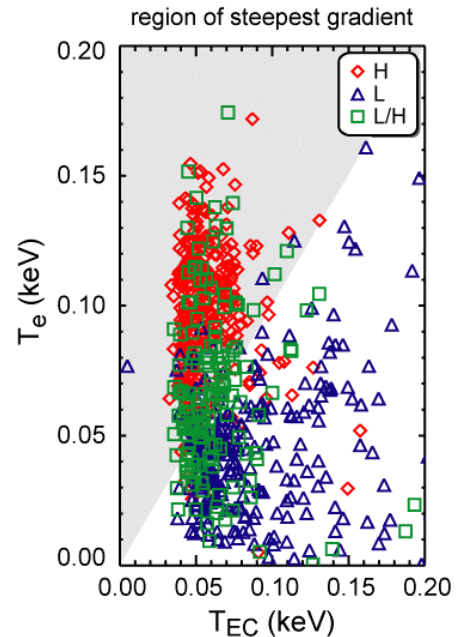

Figure 1: Comparison between experimental data from MAST and a theory for the L-H transition based on zonal flow generation by finite β drift waves. The shaded regions indicate where the theory predicts an H-mode.

than in [5], to optimise the fit to data, and this discrepancy is being investigated. The theory has also proved successful in modelling the L-H transition in DIII-D and Alcator C-MOD.

MAST data have been submitted to the ITPA L-H threshold database. Data favour a dependence of the threshold power, P_{thr} on the magnetic field at the plasma edge rather than the toroidal field on axis and with the plasma surface area, S (a function of R and a) rather than R alone [6].

2.2. The H-mode Pedestal

Even in H-modes with power levels a factor of 2 above P_{thr}, the pedestal electron temperature, T_{ped} on MAST is much lower than in comparison discharges on ASDEX Upgrade (< 0.2 keV in MAST compared to 0.5 keV in ASDEX Upgrade) [3,7], supporting a magnetic field dependence for T_{ped} observed in JET ($B_\phi^{MAST} \sim 0.45T$, $B_\phi^{AUG} \sim 2.5T$). H-mode ion and electron temperatures are typically similar in the edge of MAST and the electron density therefore dominates the pedestal pressure. A unique capability for simultaneous, high spatial resolution measurement of edge density profiles at the high and low field side in MAST has shown that the edge density width is the same in radial space on both sides but not in the normalised flux co-ordinate [7]. The lack of an impact from flux

expansion provides strong support for an analytical model of the density pedestal width developed by DIII-D, which is dependent on the neutral penetration depth [8]. The MAST data have been added to the ITPA pedestal database, where they suggest an aspect ratio dependence for the pedestal energy, $W_{\text{ped}} \propto \varepsilon^{-2.13}$ [9]

2.3. Confinement Scalings

Confinement data from quasi-steady state MAST H-mode plasmas have been merged into the international H-mode confinement database [10]. The MAST data expand the range of inverse aspect ratio (the ratio of minor to major radius, $\varepsilon = a/R$) in the database by a factor 2.2, from $0.15 < \varepsilon < 0.4$ to $0.15 < \varepsilon < 0.7$ and in toroidal β by a factor 2.5, from $0.22 < \beta < 3.5$ to $0.22 < \beta < 8.5$. The data support a slightly stronger ε dependence than indicated by the IPB98(y,2) scaling of 'engineering parameters', $\varepsilon^{0.81}$ rather than $\varepsilon^{0.58}$ but, more significantly, improve confidence by allowing data from other devices with a high leverage on ε but with non-conventional plasma cross-sections (bean-shaped and circular) to be replaced [11].
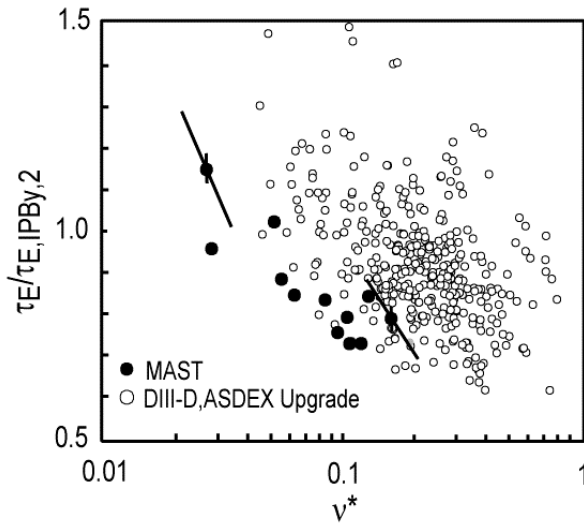

In dimensionless parameters, the addition of MAST data to the database does not significantly change the dependencies known from the IPB98(y,2) scaling: gyro-Bohm dependence on normalised Larmor radius ρ^* with β degradation. The MAST data-set alone (similar to that observed in the DIII-D and Asdex Upgrade data-sets), allows for weak favourable dependence on normalised collisionality ν^* [11] (figure 2). This discrepancy with IPB98(y,2) scaling may result from correlated errors in the data-set and requires further investigation. A quantification of this effect is especially important for scaling from the MAST data to future large ST devices, such as a Component Test Facility (CTF) [12], since the extrapolation in ν^* ($\nu^{*,\text{MAST}}/\nu^{*,\text{CTF}} \sim 90$)

Figure 2: $H_{98y,2}$ plotted against ν^* for MAST, DIII-D and ASDEX Upgrade data. The error ellipses correspond to ± 10 and ± 12 % errors on net input power and stored energy respectively.

dominates that in β and ρ^* ($\beta^{\text{MAST}}/\beta^{\text{CTF}} \sim 0.4$, $\rho^{*,\text{MAST}}/\rho^{*,\text{CTF}} \sim 0.9$). This makes predictions sensitive to errors in the scaling with ν^*. In addition MAST data provides a strong link between dependencies on β and ε. As a consequence, a scaling constrained to be β independent (in order to align with dedicated dimensionless scans) should be compensated by a change in dependence on ε, for example the recently discovered interaction between β and ν^* exponents in a dimensionless scaling [13] should also include ε.

A comparison of τ_E in closely matched L and H-mode plasmas, which is possible in MAST by a small shift away from connected double-null (CDN) operation, with predictions from the IPB98(y,2) and IPBL97 [10] scalings suggests that the ε independence in the L-mode scaling should be reviewed.

3. Heat and Particle Transport

3.1. Transport at the edge

Low aspect ratio also makes MAST ideal for studying anomalous particle, heat and momentum transport in the presence of sources and sinks. The B2SOLPS5.0 code has now

been fully implemented for studies of the boundary, scrape-off layer and divertor in MAST double-null plasmas. In L-mode, the neo-classical ion heat flux at the edge is found to be comparable with the anomalous radial ion heat flux, while neo-classical contributions to the particle and electron heat fluxes are negligible [14]. The radial electric field in the vicinity of the separatrix is always close to the neo-classical value on MAST, as previously found for ASDEX Upgrade [15].

3.2. Core transport

Core transport analysis in MAST using the TRANSP code [16,17] now regularly exploits high spatial and temporal resolution radial profiles of Z_{eff}, T_e, n_e and T_i (in the most recent campaign). Considerable care is taken to validate guiding-centre estimates for neutral beam heating, current drive and momentum input in TRANSP by comparing with the full gyro-orbit code LOCUST. This is particularly important for counter-NBI plasmas, where the prompt losses arising from the large Larmor radius for fast ions in MAST may account for up to 70% of the beam power in the low current plasmas used so far. Comparisons of TRANSP analyses for 'similar' discharges in various confinement regimes (L-mode, H-mode, ITB) and gyro-kinetic micro-stability analyses using the GS2 Code [18,19] are helping to improve understanding of the key mechanisms underlying transport in MAST from a fundamental standpoint.

3.2.1 L/H comparison discharges

TRANSP analysis of ELMy H-mode plasmas has been compared to that for L-mode plasmas. The plasmas were neutral beam heated, quasi steady state and sawtooth-free and matched as closely as possible in shape, plasma current and density [20]. In both cases, the TRANSP results are most likely to be accurate in the region of normalised radius $\rho < 0.8$, where the profiles are least affected by ELMs and experimental errors, and for $\rho > 0.3$, to avoid the impact of poor gradient resolution in the flatter profiles near the axis.

In the region $0.3 < \rho < 0.8$ of the H-mode plasma, the electron heat diffusivity, χ_e is found to be within a factor 2-3 of the ion neo-classical level, χ_i^{NC} ($\sim 1 - 2$ m^{2}s^{-1}) rising by a factor 4 for the region outboard of $\rho \sim 0.6$. For $\rho > 0.4$ the ion diffusivity, χ_i is roughly equal to χ_i^{NC}. In contrast, for the L-mode plasma both χ_i and χ_e are a factor 4 to 10 larger than χ_i^{NC} ($\sim 0.5 - 1$ m^{2}s^{-1}) over the whole profile. Nevertheless, the absolute magnitude of χ_e is similar to the H-mode for $\rho > 0.5$ and χ_i is only significantly larger than in H-mode right at the edge, $\rho > 0.7$. The relatively modest diffusivity may be consistent with at least some MAST L-mode plasmas actually having a weak internal transport barrier (ITB), a hypothesis which is supported by the high global confinement observed in some sawtooth-free L-modes ($H_{98,y2} \sim 0.8$) and the similarity of $\chi_{i,e}$, **ExB** flow shear and ITG growth rate profiles in co-NBI discharges exhibiting a clear ITB (see section 3.2.2).

Linear stability calculations for ITG modes in MAST plasmas with significant neutral beam heating have been conducted using the GS2 code [18,19]. The analysis suggests that ITG's are unstable on all flux surfaces and that mixing length estimates neglecting toroidal rotation are capable of explaining the observed χ_i ($\chi_i^{ITG} \sim 3 - 5$ m^{2}s^{-1}). The analysis also shows, however, that toroidal plasma rotation, v_ϕ in these plasmas (typically $\sim$100kms^{-1}, Mach number $M_\phi \sim 0.4$ on axis) can dominate the equilibrium pressure-driven flow shearing rate, suppressing the ITG growth rate, γ_m^{ITG}. A comparison has been made for both the L and H-mode plasmas of the **ExB** flow shear, ω_{SE} from TRANSP (which includes both the pressure-driven and toroidal rotation components) with a simple model for γ_m^{ITG}. The model is suitable for the low magnetic shear conditions that apply over most of the plasma

cross-section and agrees remarkably well with estimates from GS2. The comparison confirms that in both L and H-mode, χ_i is significantly reduced in the region where $\omega_{SE} > \gamma_m^{ITG}$.

In contrast to the ITG analysis, mixing length estimates for χ_e based on linear analysis for ETG modes yield $\chi_e^{ETG} \sim 0.1 \ \mathrm{m^2 s^{-1}}$, far below the values derived by TRANSP. Non-linear, collisionless ETG calculations for the same MAST plasma have therefore been performed in flux-tube geometry, assuming adiabatic ions [21,22]. These calculations predict the formation of radially extended streamers in the electrostatic potential with radial widths up to ~100 times the electron Larmor radius (i.e. ~1cm). Convergence tests have been conducted and the results appear robust to variations in the dimensions of the flux tube, predicting a value for $\chi_e \sim 10 \ \mathrm{m^2 s^{-1}}$, which is much closer to the TRANSP estimates.

3.2.2. Co-NBI/Counter-NBI ITB comparison discharges

In addition to H-modes, regimes with strong internal transport barriers (ITBs) are also routinely accessed in MAST, both with NBI parallel (co-) and anti-parallel (counter-) to the plasma current at the tangency radius. In both cases the central magnetic shear, q' from TRANSP is around zero or slightly negative and the transport barrier forms just outboard of this region, where q' becomes positive. The TRANSP estimate for q' is believed to be rather accurate for MAST as the resistivity is essentially neo-classical, at least for sawtooth-free discharges, being well described by the formulation of Sauter et al [23,24].

Ion-ITBs are formed with co-NBI and TRANSP analysis indicates that χ_i falls to parity with $\chi_i^{NC} (\sim 1-2 \ \mathrm{m^2 s^{-1}})$ in the vicinity of the barrier, $\rho \sim 0.5$, which is around the maximum of ω_{SE}. χ_e also falls in the same region, to roughly twice χ_i^{NC}. Profiles of ω_{SE} and γ_m^{ITG} in the co-NBI ITB discharges are remarkably similar to those derived for L-mode, with ω_{SE} dominating γ_m^{ITG} for $\rho < 0.5$ [20].

For counter-NBI discharges an electron-ITB is encountered, with a strongly peaked density profile, a broad temperature profile and an exceptionally steep electron temperature gradient at high normalised radius, $\rho \sim 0.7$. χ_e falls to roughly twice $\chi_i^{NC} (\sim 0.8 \ \mathrm{m^2 s^{-1}})$ in the barrier region. Density turbulence is significantly suppressed in these discharges, which are also characterised by very rapid toroidal rotation $v_\phi \sim 300 \mathrm{kms^{-1}}$, $M_\phi \sim 0.8$ on axis. A strong correlation is observed

Figure 3: $H_{98y,2}$ versus toroidal rotation frequency at r/a=0.5 for discharges with NBI co- and counter- to the plasma current.

on MAST between v_ϕ and normalised confinement, with the fast rotating counter-NBI discharges exhibiting the highest normalised confinement so far observed in MAST, $H_{98,y2} > 1.6$ [25] (figure 3).

The density peaking is well modelled as the cumulative effect of the Ware pinch (which is higher in counter-NBI due to an increased Z_{eff}) and a much smaller pinch term from the beam driven current (which is inwards for counter-NBI). Modelling with the LOCUST code shows that the high toroidal velocity probably results from beam momentum injection, which is
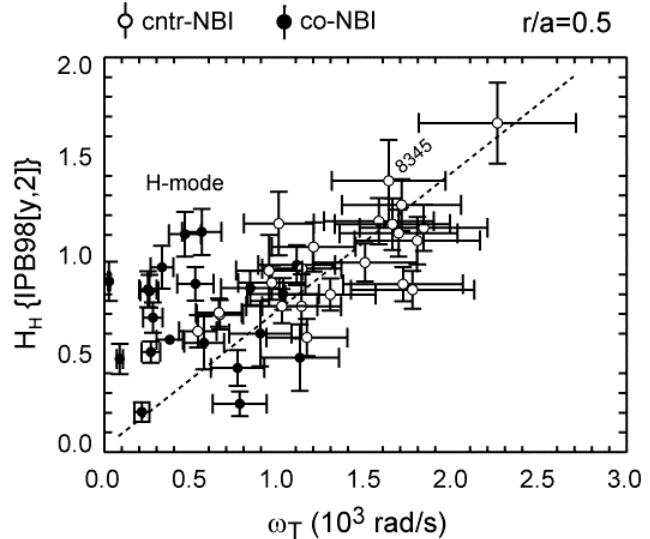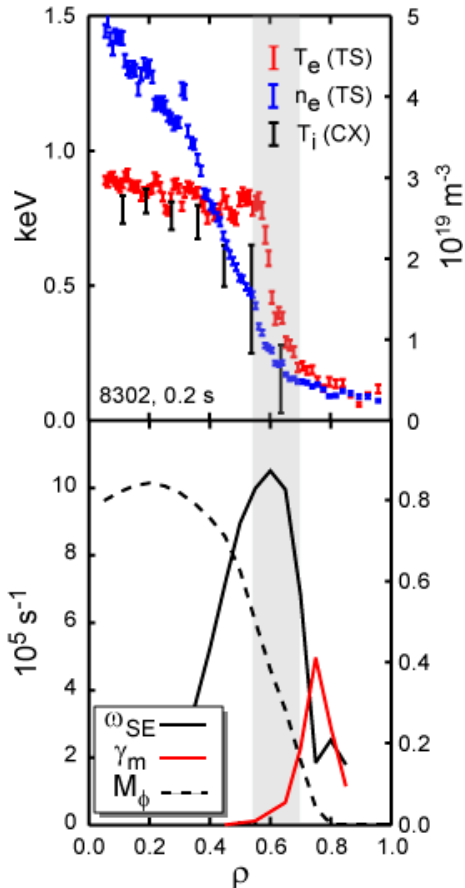
Figure 4: n_e, T_e and T_i profiles (top), rotation profile (Mach number, M_ϕ), **ExB** shearing rate, ω_{SE} and ITG growth rate, γ_m (bottom) for a counter-NBI internal transport barrier.

much higher in counter-NBI than co-NBI [25]. The enhanced torque on the plasma in counter-NBI discharges is due to the effect of large first orbit losses from the co-orbit of the fast-ion trapped particle population and is well correlated to estimates of v_ϕ derived from analysis of asymmetries in the density profile. For these plasmas, ω_{SE} exceeds γ_m^{ITG} for $\rho < 0.7$ and is a factor 20 larger at $\rho \sim 0.6$ (figure 4). Indeed ω_{SE} approaches 1.1×10^6 s^{-1} at its peak, comparable with estimates of the *ETG* growth rate from GS2, raising the possibility that both ITG and ETG turbulence could be stabilised in these plasmas. Despite ITG (and possibly ETG) stabilisation across much of the plasma radius, the ion and electron temperature profiles inside the barrier are almost flat. This is indicative of rapid transport rather than the low diffusivity one might expect. Unstable tearing parity modes have been found in GS2 calculations for the core region of MAST H-mode plasmas [19], and may be a possible candidate to explain the poor core confinement.

The MAST data strongly support the hypothesis [25] that toroidal rotation, driven by the beam torque, gives rise to a dominant contribution to the radial electric field, E_r via the $v_\phi B_\theta$ term. E_r is further augmented by the pressure gradient term. Micro-turbulence is then decorrelated and transport suppressed in regions of large **ExB** flow shear.

4. Transient Phenomena and Energetic Particle Modes

4.1. ELM Structure

The study of transient phenomena such as edge localised modes (ELM) and disruptions is a key topic for MAST, where the good diagnostic access of the ST has proved invaluable. Wide-angle images of the whole plasma in visible light from a fast 2D imaging system reveal the presence of filamentary structures in the earliest phase of ELMs [26,27]. These filaments have a toroidal mode number in the range $8 < n < 14$ and appear to follow approximately field lines with a safety factor in the range $4 < q < 6$ (roughly q_{95} in a typical MAST plasma). The filaments protrude beyond the separatrix and are clearly observed in the ion saturation current to the mid-plane, low field side reciprocating probes on MAST up to 20 cm remote from the plasma edge. The ion saturation current during each ELM, I_{sat} is separated into several distinct peaks, consistent with the motion of a series of filaments past the probes.

Simple modelling of I_{sat} for each of the probes, which are toroidally separated by 30º, at a range of radial locations is consistent with the imaging data and indicates that the filaments accelerate outboard of the separatrix at $5 - 15 \times 10^6$ ms^{-2}, reaching typical velocities of $1 - 2$ kms^{-1}. The modelling also suggests that the filaments rotate toroidally past the probes with the same distribution of velocities as experimentally observed in the MAST H-mode edge plasma, using a spatially resolved helium injection Doppler diagnostic [28]. In fact, these measurements indicate a significant toroidal velocity shear (1.8×10^6 s^{-1}) in the edge

plasma prior to the beginning of the ELM. However, this shear effectively vanishes at the ELM and the edge plasma, outboard of the pedestal, rotates at a uniform velocity of around $12 \, kms^{-1}$ (figure 5). This absence of strong velocity shear in the edge may also explain how the filaments are able to protrude beyond the separatrix without being destroyed.

The observations of ELM structure on MAST, supported by related evidence from JET and comparison studies on ASDEX Upgrade, provide strong support for a model of edge localised modes derived from a theory for the non-linear evolution of ballooning modes [29]. This theory predicts an explosive growth of ballooning instabilities, even close to the linear marginal stability boundary, which develop into highly elongated filaments extended along magnetic field lines. The filaments narrow and twist to push between field lines on neighbouring flux surfaces on the low field side

Figure 5: Toroidal velocity versus time from the peak of mid-plane D_α emission of an ELM for different radial chords at the edge, collated from a series of similar ELMs.

but remain unperturbed from their original location far along the field line. MHD stability analysis of typical MAST H-mode equilibria, conducted using the ELITE code, indicates that intermediate-n ($n \sim 6$) peeling-ballooning modes are a likely candidate for the ELM trigger in MAST.

4.2. Disruption Power Loads

The release of energy from the core plasma during disruptions and the resultant heat load on plasma facing components have been explored on MAST as part of research co-ordinated by the EU Plasma-Wall Interaction Task Force [30]. Disruptions triggered by the growth of a locked mode in low density, high β_{pol} discharges and vertical displacement events (VDE), triggered by deliberate termination of the plasma position vertical feedback, have been studied.

Data from a high spatial and temporal resolution IR camera, with wide-angle views of the divertor and first wall, indicate that the evolution of disruption heat loads is more complex than previously thought [31]. In both locked mode and VDE disruptions around 30-40% of thermal plasma stored energy, W can be released in the period immediately prior to the beginning of the current redistribution (characterised by a rapid rise in the plasma current). In the locked mode case this period is typically 6-20 ms, a significant fraction of the energy confinement time for these plasmas $\tau_E \sim 50ms$, but is much more rapid for the VDE, 2-5 ms. During this phase, the target heat flux width, Δ_H remains approximately constant and peak power loads rise by a factor 2-5 for the locked mode and a factor 10 for the VDE. The explanation for this core energy loss in each case is not yet clear and is being investigated. Similar behaviour has, however, been observed on JET [30].

The plasmas studied were close to a double-null divertor configuration prior to the disruption, with roughly balanced power to the upper and lower targets (and overwhelmingly to the low field side). This power balance is maintained in the early phase but is lost in the period immediately following the beginning of current redistribution, with energy released from the core arriving predominantly to one or other target. This phase is much faster, with the
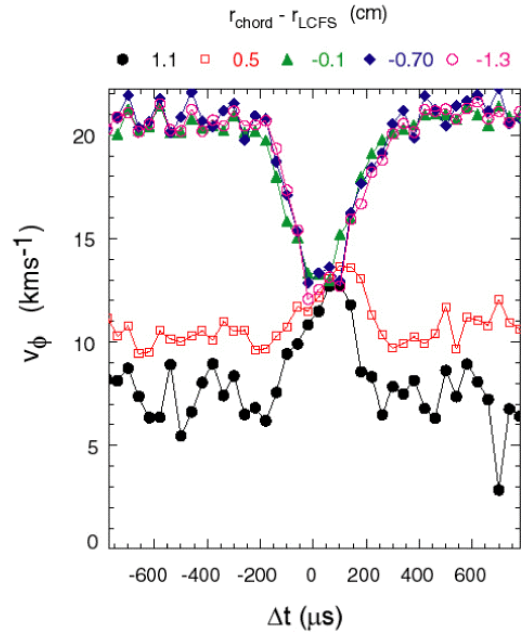
remaining 60-70% of *W* being released in ~2.2 ms for the locked mode disruptions and in only ~750 μs for the VDE. Naturally, the target power load rises significantly during this phase, however the rise is substantially ameliorated by a significant broadening of Δ_H. In the locked mode case, Δ_H increases from ~5 cm in the pre-quench to an average of around 40 cm, keeping the rise in peak heat flux to less than a factor 2 over the earlier phase (figure 6). Importantly, however, the energy deposition is highly non-uniform, both poloidally and toroidally, with localised 'hot-spots' and some regions receiving little heat flux.

Figure 6: Target power loads at two times with respect the disruption, ~3ms prior to the peak in the plasma current (end of the current redistribution) (dotted line) and <1ms before (solid line).

4.3. Energetic Particle Modes

Energetic particle driven modes are predicted to play an important role in determining the efficiency of α-particle heating in future devices. The low toroidal magnetic field of the ST makes MAST a good test bed for studying energetic particle modes (EPM) at high normalised plasma pressure, *β,* due to the super-Alfvénic nature of the neutral beam injection (NBI). For typical MAST conditions (toroidal field, $B_\phi \sim 0.5$T, electron density, $n_e \sim 3 \times 10^{19}$m^{-3}) the Alfvén velocity, $v_A \sim 1.4 \times 10^6$ms^{-1} is significantly less than the velocity of deuterium ions at the full neutral beam energy in MAST, $v_{NBI} \sim 2.1 \times 10^6$ms^{-1}. Alfvén waves are therefore readily excited via the fundamental resonance with the parallel component of the beam ion velocity $v_{//,NBI} \sim 0.7 v_{NBI} \sim v_A$. Toroidal (TAE) and elliptical (EAE) Alfvén eigenmodes and chirping modes are all clearly observed on MAST [32].

At low densities and high temperatures the TAE activity occasionally gives rise to frequency-sweeping modes, in which up-frequency and down-frequency chirping is simultaneously observed [32] (figure 7). The observation of these modes has provided support for a model for the non-linear evolution of TAE's in the 'explosive' regime, which predicts the formation of Bern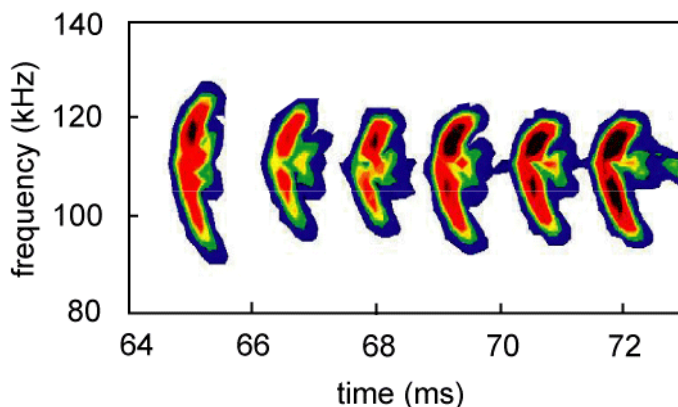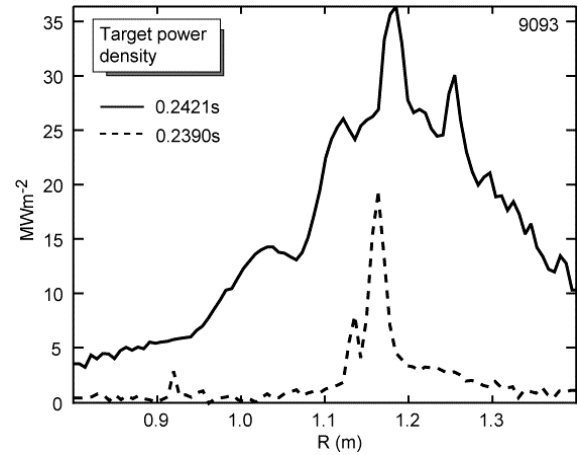stein-Green-Krushal (BGK) non-linear waves [33]. Modelling of the modes using the HAGIS code [34] has allowed the absolute magnitude of the TAE perturbation to be estimated from the frequency-sweeping rate. For discharges with β > 5% the TAE and EAE activity is reduced and the Alfvén instabilities become dominated by down-frequency chirping modes, with a much larger fractional frequency shift (δω/ω ~ 50%) than the frequency-sweeping modes (δω/ω ~ 20%). The mode amplitude of these non-perturbative EPMs falls sharply with increasing β and vanishes for β > 15%, suggesting that TAE, EAE and chirping activity are all likely to be absent in a future ST device where β on axis would approach 100%. The impact of other EPM

Figure 7: Spectrogram of frequency-sweeping modes observed in MAST, shot #5568

instabilities (e.g. fish-bone and compressional Alfvén eigenmodes) at high β is still to be determined.

5. Start-up, Sustainment and Exhaust

5.1. Start-up without a central solenoid

Due to the requirement for neutron shielding (of all coils, normal or super-conducting), future large ST devices operating with a DT-mix would be unlikely to retain sufficient space in the centre column for a useful solenoid. Schemes enabling effective plasma start up without a solenoid are therefore of particular interest to the ST. Several schemes are currently being investigated or under consideration, including co-axial helicity injection on NSTX [35] and various RF methods on CDX-U, DIII-D [36] and MAST [37]. So-called 'merging-compression' has been extensively studied and successfully employed on both MAST and its predecessor START. In this scheme plasma breakdown occurs around each of a pair of internal 'induction' coils, the separate plasma rings merge towards the vessel mid-plane to form closed flux surfaces as I_p builds-up and the plasma is compressed towards the centre column by an increasing vertical field, further increasing I_p. Unfortunately internal coils will be difficult or impossible in a future device. However a variant of this method, Double Null Merging (DNM) may be applicable. DNM was previously used on START and is now being developed, in association with ENEA-Frascati, for use on MAST. Initial tests have been very successful.

Figure 8: Plasma current traces for two plasma created by DNM, with zero current in the central solenoid - with (solid line) and without (dotted line) vertical field ramping to sustain the current near the peak value.

In DNM plasma breakdown occurs at a quadrupole magnetic null formed between pairs of coils in the upper and lower divertor regions. Ramping the coil currents rapidly and in ratio increases the current in the plasma 'rings' whilst maintaining a static null. When the plasma current is sufficiently high and the coil current has fallen towards zero, the rings move towards the mid-plane where they merge forming closed flux surfaces. Using the DNM start-up scheme, a tokamak plasma with I_p up to 370kA has been formed in MAST without current in the central solenoid. Core electron temperatures and densities were measured at 0.4 – 0.6 keV and 1.5 - 9x10^{19}m^{-3} respectively. Ramping the vertical field coils during and after the merging allows I_p to be maintained close to the peak value for >50 ms. Future experiments will use this plasma as a target for RF heating and current drive, to develop a solenoid independent plasma start-up and sustainment scenario. Existing, internal coil sets were used to demonstrate DNM in these experiments. Importantly, however, the plasma forms at the magnetic null and not around the coils themselves, as occurs with merging-compression. This would make it feasible to use coils external to the vessel, as would be required in a future device.

5.2. Error Field Studies

Development of a stable, low density plasma target for studies of neutral beam current drive in MAST have been hampered in the past by an intrinsic error field, leading to the formation
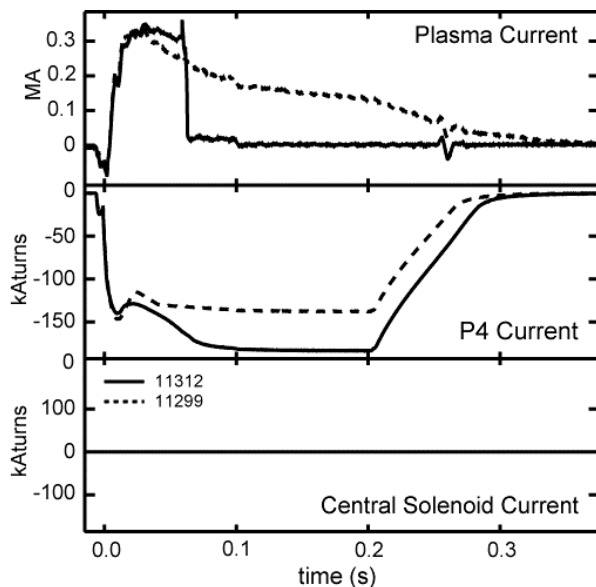
of a plasma terminating locked mode. A set of error field compensation coils (EFCC) has recently been installed to address this problem and to enable studies of the impact of error fields in the ST. The EFCC comprises two orthogonal sets of 15kAturn Helmholtz coils, capable of producing a magnetic field with 2:1 structure of up to 6.8×10^{-4} T at the $q = 2$ surface of a typical plasma.

Preliminary experiments have demonstrated that the EFCC can successfully compensate for error fields in both Ohmic and neutral beam heated plasmas and eliminate the growth of locked modes at low density. In the Ohmic case, it was possible to extend the operational space to the lowest density achievable without active pumping (i.e. that determined by recycling in the absence of additional gas puffing). Studies have been conducted using the EFCC to determine the scaling of the error field amplitude necessary to induce a locked mode with B_ϕ, n_e and q_{95}. The MAST data shows an approximately linear dependence of the error field threshold on plasma density and a weak dependence on torodial field, similar to the scalings found on JET and DIII-D [10]. Comparison of the MAST data with that from the other devices should allow an aspect ratio scaling for this ratio to be determined in the future.

5.3. Divertor Biasing

Handling of the divertor target heat flux is a known challenge for future devices. The issue is of particular note for large ST devices, due to the reduced major radius and thus wetted area in the divertor over which power is deposited. Several novel schemes are being explored first in the current generation of ST's but are of equal interest to future, large conventional aspect ratio devices. These include techniques such as 'dynamic' plasma facing components formed, for example from a cascade of mm-scale pebbles (of silicon carbide or other material) or from liquid lithium. One alternative technique which has been investigated on MAST is the use of toroidally asymmetric electrical biasing of divertor components to broaden the target heat flux width, increasing the wetted area [38].

The MAST divertor is naturally separated into twelve toroidal segments. Six of these, alternating toroidally, are isolated from the vessel and can be connected to a biasing power supply capable of delivering up to 5 kA at 120 VDC. For bias potentials above 80 V, the total current to the biased elements remains approximately constant, at 3-5 kA for typical conditions. The biasing generates a toroidally 'wavy' wetted area, which is an explicit prediction of the theory for divertor biasing. This perturbation is a product of the **ExB** drift between the toroidal magnetic field in the vessel and the electric field imposed between SOL flux tubes by biasing (the field being in opposite directions at the biased and grounded ribs). The results validate other aspects of the theory, which predicts that biasing should generate convective ion motion, with localised broadening of the heat flux width in the scrape-off layer (SOL) of the divertor region. In recent experiments, a reduction in peak heat flux at the divertor target of 75% was observed using the divertor IR, concomitant with a factor 4 increase in heat flux width. An understanding of the impact of imposing a controlled electric field on the divertor may also contribute in future work to an improved understanding of SOL turbulence.

6. Conclusions

Significant progress has been made on MAST towards development of a first principles based understanding of transport, stability and edge physics. The magnetic geometry of the ST; low B_ϕ, high toroidicity, large ε, high β, strong shaping and so on, coupled with the excellent diagnostic access on MAST has provided many opportunities to test both models and theories under extreme conditions. Comparison studies with other ST and conventional aspect ratio devices and integration of MAST data into international databases has proved

especially beneficial, allowing the explicit impact of key parameters such as B_ϕ and ε to be determined. Progress has also been made towards developing regimes on MAST that will contribute towards demonstration of fully non-inductive plasma start-up and sustainment, a key goal for the ST.

Acknowledgements

References

[1] H. Meyer *et al*, "The effect of magnetic configuration on H-mode in MAST", Proc. 29th EPS Conf. on Plasma Phys. and Control. Fusion (2002)
[2] R. Akers *et al*, Phys. Plasmas 9 (2002) 3919
[3] H. Meyer *et al*, this conference
[4] H.R.Wilson, P.B. Snyder, G.T.A. Huysmans and R.L. Miller, Phys. Plasmas 9 (2002) 1277
[5] P.N. Guzdar *et al*, Phys. Rev. Lett. 89 (2002) 265004
[6] Y. Martin *et al*, this conference
[7] A. Kirk et al., Plasma Phys. Control. Fusion 46 (2004) A187
[8] R.J. Groebner R J *et al*, Plasma Phys. Control. Fusion 44 (2002) A265
[9] G. Cordey *et al*, Nucl. Fusion 43 (2003) 670-674
[10] ITER Physics Basis, Nucl. Fusion **39** (1999) 2204
[11] M. Valovic *et al*, this conference
[12] H Wilson *et al*, 31st EPS Conf. ECA**28**G (2004) P4.196
[13] G. Cordey at al, this conference
[14] V. Rhozansky, G. Counsell and A. Kirk, "Simulation of Neoclassical Effects with B2SOLPS5.0 for MAST", Proc. 31st EPS Conf. on Plasma Phys. and Control. Fusion (2004)
[15] V. Rozhansky *et al*, Nucl. Fusion, 42 (2002) 1110
[16] R.J. Hawryluk, in Proc. of the Course in Physics Close to Thermonuclear Conditions, Varenna, (Commission of the European Communities, Brussels), Vol. I, 19 (1980).
[17] A. Pankin et al., Computer Physics Communications, **159**, 3, 157 (2004).
[18] M. Kotschenreuther, G. Rewoldt and W.M. Tang, Computer Physics Communications 88 (1995) 128
[19] D.J. Applegate *et al*, "Microstability in a spherical tokamak 'MAST-like' high confinement mode equilibrium", to appear in Phys. Plasmas (2004)
[20] A.R. Field *et al*, this conference
[21] C.M. Roach *et al*, Proc. Theory of Fusion Plasmas, Joint Varenna-Lausanne International Workshop
[22] N. Joiner *et al*, Proc. 31st EPS Conf. on Plasma Phys. and Control. Fusion (2004)
[23] Sauter O *et al* 1999, *Phys. Plasmas* **6** 2834.
[24] Sauter O *et al* 2002, *Phys. Plasmas* **9** 5140.
[25] R. Akers *et al*, this conference
[26] A. Kirk *et al*, Phys. Rev. Lett. 92 (2004) 245002
[27] A. Kirk *et al*, "Structure of ELMs in MAST", submitted to Plasma Phys. Control. Fusion.
[28] A. Kirk *et al*, this conference.
[29] H.R. Wilson, S.C. Cowley, Phys. Rev. Lett. 92 (2004) 175006
[30] A. Loarte *et al*, this conference
[31] G.F. Counsell and F. Lott, "Distribution of thermal energy during disruptions on MAST", Proc. 31st EPS Conf. on Plasma Phys. and Control. Fusion (2004)
[32] M. Gryaznevich, S. Sharapov, PPCF 46 (2004) S15-S19
[33] H.L. Berk, B.N. Briezmann and N.V. Petviashvili, Phys. Lett. A234 (1997) 213
[34] S.D. Pinches *et al*, Computer Physics Communications 111 (1998) 133
[35] "Co-axial helicity injection in NSTX"
[36] C. Forest, Phys. Plasmas, 1 (1994) 1568
[37] V. Shevchenko *et al*, "EBW Current Drive Start-up Scenario for MAST", Proc. 31st EPS Conf. on Plasma Phys. and Control. Fusion (2004)
[38] G.F. Counsell *et al*, "Reduction of Divertor Power Loading in MAST", Proc. 30th EPS Conf. on Plasma Phys. and Control. Fusion (2003)